Programmable Jigsaw Puzzles of Soft Materials Enabled by Pixelated Holographic Surface Reliefs

Yifei Wang, Cong-Long Yuan, Wenbin Huang, Pei-Zhi Sun, Binghui Liu, Hong-Long Hu, Zhigang Zheng, Yan-Qing Lu,* and Quan Li**

Manual intervention in the self-organization of soft matter to obtain a desired superstructure is a complex but significant project. Specifically, optical components made fully or partially from reconfigurable and stimuli-responsive soft materials, referred to as soft photonics, are poised to form versatile platforms in various areas; however, a limited scale, narrow spectral adaptability, and poor stability are still formidable challenges. Herein, a facile way is developed to program the optical jigsaw puzzle of nematic liquid crystals via pixelated holographic surface reliefs, leading to an era of manufacturing for programmable soft materials with tailored functions. Multiscale jigsaw puzzles are established and endowed with unprecedented stability and durability, further sketching a prospective framework toward customized adaptive photonic architectures. This work demonstrates a reliable and efficient approach for directly assembling soft matter, unlocking the long-sought full potential of stimuli-responsive soft systems, and providing opportunities to inspire the next generation of soft photonics and relevant areas.

1. Introduction

A jigsaw puzzle is an interesting activity that requires assembling numerous pieces containing specific colors and contrasting information into fascinating and completed pictures. Recently, scientists have leveraged various types of jigsaw puzzles as a versatile block to establish numerous ingenious applications, such as supramolecular engineering,[1] nanotechnology,[2] soft robotics, and mechanical metamaterials.[3,4] When scaling down the size of each piece of the jigsaw puzzle and extending the concealed information to contain both light polarization and phase, the concept of optical jigsaw puzzles aiming for programmable optics can be obtained. It is known that the functions of traditional optical elements are endowed by a complex phase wavefront, e.g., an imaging lens has a parabola-shaped phase distribution, and a grating has a periodic phase distribution,[5,6] and are expressed using the curved interface between different optical materials in geometrical optics. Metasurfaces,[7,8] composed of pixelated nanoantennas with different parameters of orientation, size, aspect ratio, spacing, etc., to obtain delicate control over the optical phase, polarization, or amplitude, have attracted tremendous scientific and industrial interest. However, these materials face the challenges of limited size, complicated microfabrication, and the dynamic manipulation of optical performance, which are the main obstacles to promoting the commercialization of smart, adaptive, and programmable photonics.

Y. Wang, C.-L. Yuan, P.-Z. Sun, B. Liu, Z. Zheng
School of Physics
East China University of Science and Technology
Shanghai 200237, China
E-mail: zgzheng@ecust.edu.cn

Y. Wang, C.-L. Yuan, P.-Z. Sun, B. Liu
School of Materials Science and Engineering
East China University of Science and Technology
Shanghai 200237, China

W. Huang
School of Optoelectronic Science and Engineering and Collaborative Innovation Center of Suzhou Nano Science and Technology
Soochow University
Suzhou 215006, China

H.-L. Hu
School of Chemistry and Molecular Engineering
East China University of Science and Technology
Shanghai 200237, China

The ORCID identification number(s) for the author(s) of this article can be found under https://doi.org/10.1002/adma.202211521.

DOI: 10.1002/adma.202211521

Y.-Q. Lu
National Laboratory of Solid State Microstructures
Key Laboratory of Intelligent Optical Sensing and Manipulation
Collaborative Innovation Center of Advanced Microstructures and College of Engineering and Applied Sciences
Nanjing University
Nanjing 210093, China
E-mail: yqlu@nju.edu.cn

Q. Li
Institute of Advanced Materials and School of Chemistry and Chemical Engineering
Nanjing 211189, China
E-mail: quanli3273@gmail.com

Q. Li
Advanced Materials and Liquid Crystal Institute and Materials Science Graduate Program
Kent State University
Kent, OH 44242, USA

Soft material, exhibiting interesting phenomena such as supramolecular architecting,[9] bio-compatibility,[10] self-assembly, and stimuli-responsiveness,[11,12] has the fascinating capability to create an incredible range of complex superstructures on multiple length scales that can perform unexpected functions. Liquid crystals (LCs) are typical soft materials with both fluidity and molecular order and can self-organize into complex hierarchical superstructures depending on molecular cooperative effects and boundary anchoring conditions.[13–15] The directed and programmable manipulation of these LC blocks to establish desired optical jigsaw puzzles with coupled functionality toward practical applications is being intensely investigated by scientists; this requires a delicate harmonization of factors including surface condition, interface energy interplay, system entropy and stimuli driving dynamics. Among various approaches to generate desired jigsaw puzzles, traditional mechanical techniques, such as surficial rubbing, nanoimprinting, and nanoscratching, are not applicable owing to the sophisticated fabrication and limited degrees of freedom in facilitating LC orientation programming.[16–18] Some photochemical approaches have been proposed to direct the rational organization of LCs, thereby enabling novel functionalities and matching the burgeoning requirements of modern science and technology.[19–22] By these means, LC optical jigsaw puzzles, typically based on the Pancharatnam-Berry (PB) phase, offer a powerful route to control light propagation via reflection,[23] scattering,[24,25] and phase modulation,[26,27] supplying a versatile strategy to achieve a fascinating planar, compact and integrated system with impressive capability in stimuli responsiveness; this architecture is referred to as "soft photonics". Nevertheless, the stability of photoresponsive materials used in photochemical approaches is a major concern from the very beginning of their development.[28] Moreover, the byproducts of photochemical reactions may also give rise to some undesirable issues.[29–32] Thus, the realization of programmable LC jigsaw puzzles to construct an arbitrary phase wavefront via a simple and low-cost process with high resolution, high efficiency, and high stability remains an urgent task.

Herein, we propose an efficient approach of directly assembling nematic LC soft blocks to facilely program a fantastic optical jigsaw puzzle using pixelated microsquare pieces covered with holographic stripe reliefs, thereby inducing LC microdomains with uniform orientation confined by pixelated surface subwavelength topography. The holographic surface reliefs are obtained via self-developed lithography, which allows precise control of the self-assembling behaviors of LCs in a digitalized manner, and the robustness of these stripe reliefs enables stable construction of highly ordered soft materials. As the realization of LC jigsaw optical puzzles originating from a delicate interplay between the LC self-assembling order and the anchoring order of holographic reliefs, the coupling among the arrangement of microscale LC domains and the anchoring conditions of holographic reliefs are further explored from different aspects, including the influence of subwavelength periodicity, structure orientation, and topography depth. To verify the versatility of LC jigsaw puzzles, diverse phase distributions have been tailored by assembling the pixelated liquid crystal domain pieces to yield the designed optical puzzles. This further allows the program of elaborate greyscale images and dynamically switchable colored patterns with LCs for the first time. Moreover, the proposed LC jigsaw puzzles also hold promise as the basis for structured lights, such as optical vortices and Airy beams, enabling multifaceted photonics techniques. This work provides a reliable way to program the self-organization of soft matter and solidifies the platform of programmable soft material for soft photonics, further unlocking the full potential of soft matter as a stimuli-responsive medium in adaptive flat optics.

2. Results and Discussion

The pixelated holographic surface reliefs are established upon self-developed digital holographic lithography (**Figure 1**a and Experimental Section) to facilely direct LC orientation and program the desired jigsaw phase pattern. The sophisticated optical setup enables a high-efficiency processing approach with unprecedented versatility and accuracy in defining the pixelated holographic surface reliefs (Supporting Information Note S1), thereby ensuring arbitrary LC phase platelets with directional topography. The stripe topography (Figure 1b,c) serves as the anchoring boundary to direct the LC arrangement,[15,33–37] and LC directors in contact with the topography will interact with adjacent directors in the bulk via a continuum coincident effect to reach a delicate equilibrium between the anchoring condition and the free energy of the system, resulting in uniform alignment along the directional reliefs (Figure 1d). Additionally, there are multiple modulation degrees of freedom when arranging the pixelated holographic reliefs, such as the directions, period, and depth (Figure S4, Supporting Information). This facilitates versatile and delicate control of the nanoscale molecular arrangement via microscopic topography, further presenting corresponding optical phenomena over the macroscopic scale with the designed LC jigsaw optical puzzles. Thus, macroscopic phenomena are bridged with mesoscale structure and nanoscale molecular self-organization.

Herein, a series of investigations are demonstrated for a further understanding of the holographic reliefs in directing LC orientation, and a commercial nematic LC with an inherent birefringence of 0.18 at room temperature is used (23 °C, 633 nm, Supporting Information Note S2). The alignment of the LC near the edges with adjacent heterogeneous orientations are detected by polarizing optical microscopy (POM) (Figure S7, Supporting Information). When the intersect angles between the directional reliefs in adjacent regions are 10°, 20°, and 45° respectively, the microscopy images show defect-free texture and appear with corresponding grey scales. There will appear boundary lines due to the disclinations between the adjacent heterogeneous orientations when the orientations of the adjacent regions vary between 0° and 90°. Besides, the regions of disclination lines would expand with the period of stripe reliefs increased, which may originate from the decreasing anchoring strength. Moving forward, the traditional LC twist angle method is used to clarify the directing capability of the pixelated surface reliefs on the LC orientation (Figure S9a, Supporting Information).[38] The results indicate that the anchoring energy exerted onto LC directors by the subtle groove topography changes between 10^{-6} J m^{-2} and 10^{-4} J m^{-2}, depending on the

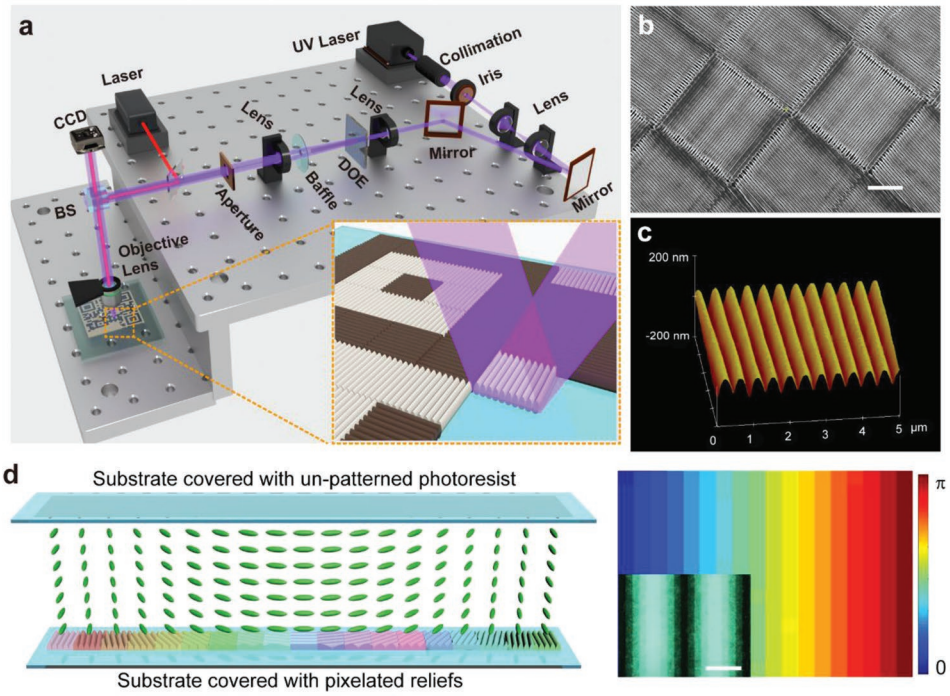

Figure 1. Direct assembly of liquid crystal optical puzzle pieces using pixelated surface reliefs. a) Schematic illustration of the self-developed digital holography lithography. The collimated and uniform pulsed ultraviolet (UV) laser beam is incident upon a 4f imaging system with a diffractive optical element (DOE) situated between the two Fourier lenses. The ±1 order diffractions are converged by an objective lens to form the interference field. The orientation of the micro/nano light field can be continuously adjusted by rotating the DOE, and the continuous modulation of the space-frequency can be realized by moving the phase grating. The inserted image illustrates the realization of the programmable jigsaw puzzles via pixelate holographic surface reliefs. BS: beam splitter. A baffle is utilized to block the zero-order residue light for better exposure. b) Scanning electron microscopy image of pixelate holographic surface reliefs. Scale bar: 10 μm. c) Atomic force microscopy image of holographic surface relief. d) Schematic and characterization of LCs orientation defined by pixelated surface reliefs. A single-side-patterned LC cell is demonstrated, where an un-patterned substrate is used as the top substrate and the directions of stripe reliefs on bottom substrate periodically vary from 0° to 180° with a step increment of 10°. The molecular orientation is confirmed experimentally with a microregional Stokes parameter test. The measured azimuthal director distribution indicated that LCs aligned as designed, and the corresponding micrograph is shown in the inset. Scale bar: 100 μm.

topographic period and depth of the stripe reliefs. That is, the anchoring strength shows a negative correlation with the period of reliefs, while is positively related to the depth, which agreed with the results of prior works.[39,40] Furthermore, the ordering of LC directors is characterized by investigating the birefringence of LC bulks, and a high birefringence value of 0.179 can be obtained (Figure S9b, Supporting Information), indicating the satisfactory ability of holographic reliefs in directing LCs. It is also noteworthy that the birefringence decreases slightly when the thickness of the bulk LC reaches a high value of 20 μm, implying the robustness of the holographic topography in defining an anchoring boundary for bulk soft materials.

The applicability of the holographic reliefs in directing the LCs toward functional jigsaw puzzles is investigated further by evaluating the electro-optical performance of a traditional twisted nematic (TN) LC achieved via pixelated reliefs. Here, the relief directions on the upper and bottom substrates are perpendicular to each other, thus inducing a 90° twist angle in the LC bulk. The electro-optical characteristic of the TN-LCs is experimentally tested using a He-Ne laser beam and is theoretically carried out based on the finite-element method (**Figure 2**a). The experimental result exhibits typical electro-optical behaviors of the normal-white TN LC and is consistent with the theoretical simulation. The cell shows defect-free bright and dark states in the OFF and ON states owing to the optical activity of the TN LCs. The results strongly suggest that the twisted orientation of the LCs has been achieved via the orthogonal reliefs as desired, thus revealing the fact that pixelated holographic surface reliefs have good applicability in directing the ordering of LCs.

Any desired jigsaw puzzle can be established by programming the LC twist angle in each pixel, thereby yielding a differently designed optical effect. For instance, a black-and-white quick response (QR) code is programmed and presented as sandwiched between two crossed polarizers (Figure 2b-I and II). A hiding and appearing QR code can be achieved by applying and removing an operating voltage of 10 V. In the same way, more complicated patterns, such as a vivid carp and dragon and phoenix with sharp and subtle edges, containing the Chinese traditional auspicious patterns are presented (Figure 2b-III,IV). Considering practical applications, a weaker driven voltage, that is, lower energy consumption is commonly desired; in addition, the information hiding in the OFF state is preferable for ensuring individual privacy. Herein, an ingenious prototype of an electrically controlled identity card with the aforementioned QR code is achieved with the assistance of an external normal-dark TN LC light valve (Video S1, Supporting Information). When the external voltage is absent, there is an information null state, exhibiting a black background (Figure 2c-I);

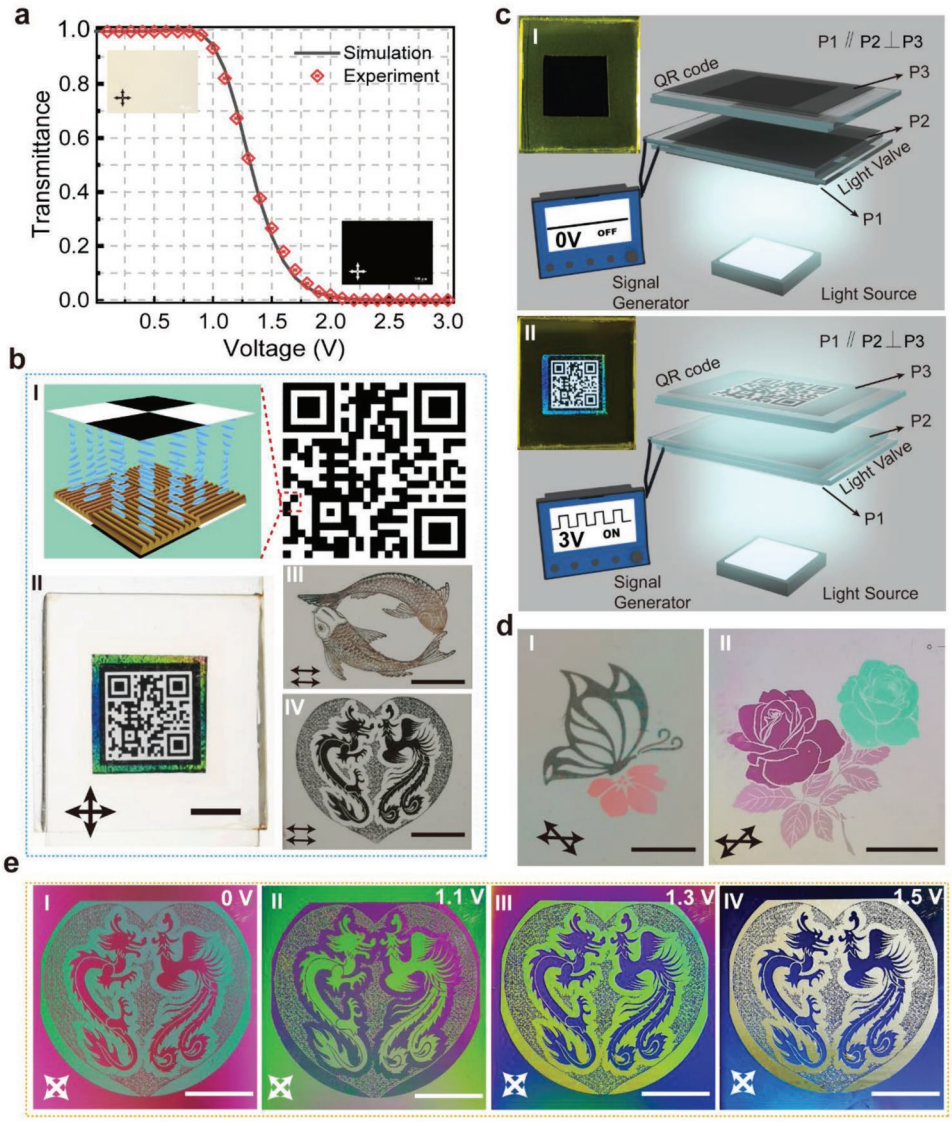

Figure 2. Jigsaw optical puzzles of LCs via pixelated holographic reliefs. a) The electro-optical characteristics of TN LC in the experimental test and theoretical simulations. The insets show polarizing optical micrographs of the TN LC in the off state (0 V) and on state (3 V). b) Black-and-white QR code pattern. I) The illustration on the left shows TN and parallel aligned (PA) liquid crystal puzzle pieces induced by programmed pixelated holographic reliefs corresponding to the region marked with a red line. II) Image of a programmed LC 2D QR code sandwiched by two orthogonal polarizers. The black and white puzzles correspond to the regions with twisted angles of 0° and 90°, respectively. The scale bar is 5 mm. III,IV) Complicated patterns of vivid carp and dragon and phoenix when the two polarizer axes are parallel, the same patterns with complementary optical effects are displayed under the crossed polarizers. The scale bar is 4 mm. c) A hidden and switchable QR code. P: polarizer. A TN LC light valve is employed to control the passage of light. I) As the external voltage is absent, the information in the QR code is hidden. II) When the light valve is turned on, the polarized light passes through the QR code, and a clear contrast between the two different regions (PA and TN) is observed (Video S1, Supporting Information). d) Colourful patterns with LC jigsaw puzzles of black wings (twisted angle: 0°) on a pink flower (twisted angle: 45°). The scale bar is 3 mm; purple (twisted angle: 60°) and green (twisted angle: 120°) petals, and light purple (twisted angle: 30°) leaves. The scale bar is 4 mm. e) Tunable birefringent colors switched with the applied voltage: I) 0 V, II) 1.1 V, III) 1.3 V, and IV) 1.5 V (Video S2, Supporting Information). The scale bar is 4 mm.

when applying the lower voltage of 3 V, the QR code, including certain security information, reappears (Figure 2c-II).

Furthermore, not only the black and white patterns but also the colorful patterns can be assembled with certain programmed jigsaw puzzles by carefully modulating the polarizer axes and the twisted angle of the LC in each pixelated puzzle (Figure 2d). Such a colorful display is ascribed to the polarization interference caused by LC birefringence, which is distinct from the previously reported structural colors and plasmonic colors generated via inorganic semiconductors or metal materials with complicated processing approaches. Impressively, such birefringence colors can also be induced by switching the applied external voltage (Figure 2e; Video S2, Supporting Information), which originates from the reorientation of LCs from their initial state. Hence, the LC jigsaw optical puzzles exhibit versatile capabilities and further provide infinite possibilities for

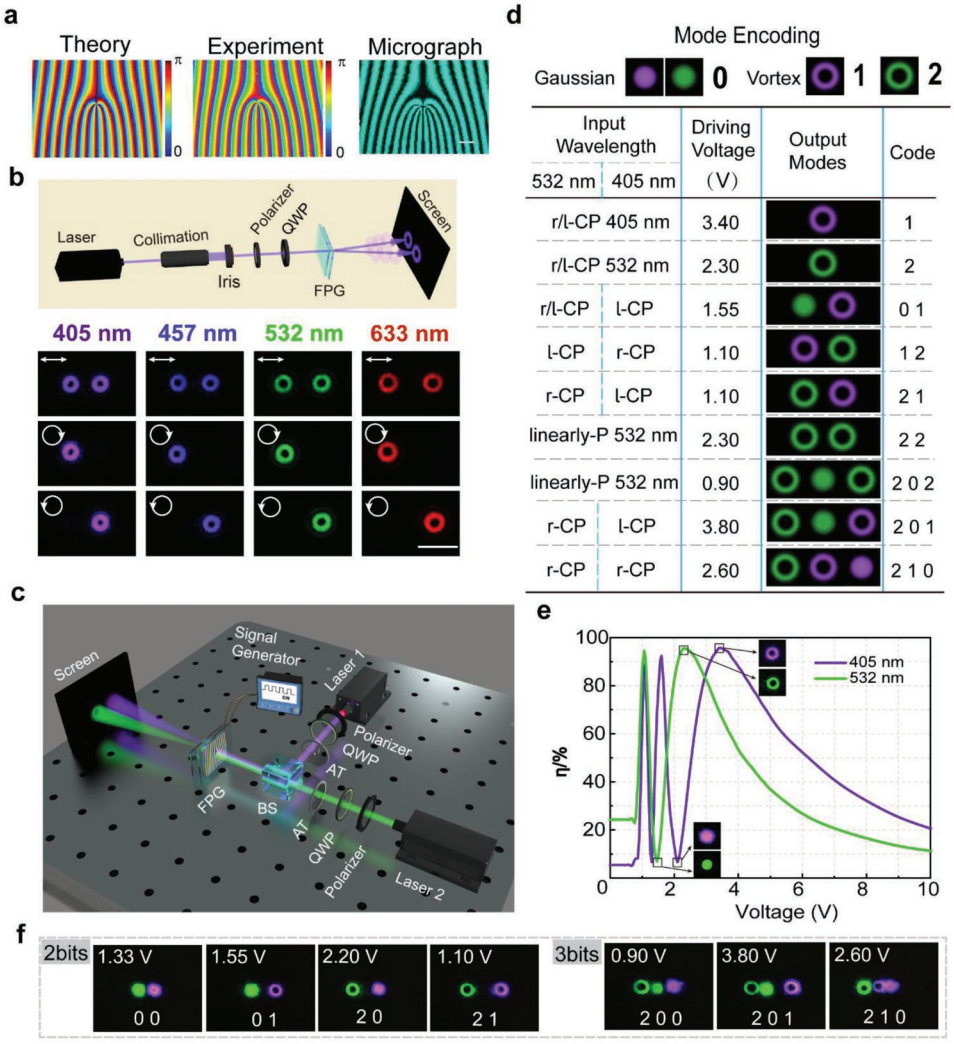

Figure 3. Planar optical elements based on LC jigsaw puzzles to generate OVs. a) The theoretical design, experimental data, and micrograph of an FPG based on LC jigsaw puzzles. The color variation from blue to red indicates the optical axis (i.e., the orientation of LCs) varying from 0° to 180°. The experimentally detected director distribution matches well with the theoretical design, while the optical texture of the POM also indicates the varying orientation of LCs. The scale bar is 200 µm. b) The optical setup for characterizing the LC FPG and the diffraction patterns with different wavelengths of 405, 457, 532, and 633 nm. Incident polarizations are labeled in the images; clockwise/counterclockwise indicates right/left circularly polarized light. The diffraction patterns are received at a distance of 90 cm. Scale bar: 5 mm. c) Optical setup for three-dimensional encoding. BS: beam splitter; AT: attenuator; and QWP: quarter-wave plate. d) Parts of ternary encoding with single-, double- and triple-bit optical signals. e) Diffraction efficiency (η) dependent on the applied voltage of the FPG at 405 and 457 nm. Here, η is defined as the intensity ratio of the diffraction order to the transmitted light. f) Experimental demonstration of 2-bit ternary coding with an applied voltages of 1.33 V (0 0), 1.55 V (0 1), 2.20 V (2 0), 1.10 V (2 1), and 3 bits ternary coding at 0.90 V (2 0 0), 3.80 V (2 0 1) and 2.60 V (2 1 0).

innovative applications, such as switchable E-tags and optical information storage,[41,42] which show promising potential for generating fade-free, environmentally friendly, and active tunable colors.

For microstructures, pixelated reliefs with small sizes are required, and the behavior near the edges becomes more relevant to the optical performance. Herein, the LC orientation and the compatibility in the edges of 16 µm × 16 µm pieces are investigated (Supporting Information Note S4). The lithography system can provide accurate control of the relief positions, allowing a continuously ordered distribution of LCs, which make the programmable jigsaw puzzle a promising candidate for planar optics, where each piece of the LC jigsaw optical puzzle is elaborately designed and loaded with the corresponding phase information. To further confirm the feasibility of LC-based jigsaw puzzles, planar photonic devices with interesting and complex functions are programmed and demonstrated. The hologram used to generate a polarized optical vortex (OV) with a topological singularity embedded into the polarization grating is assembled with LCs, forming a fork-shaped phase topography (**Figure 3**a).[43,44] Additionally, the performance of such a forked polarization grating (FPG) is characterized by the optical setup illustrated in Figure 3b. The prominent donut-like OVs with four typical wavelengths of 405, 457, 532, and 633 nm are received at the black screen by switching the external applied voltage (Figure 3b;

Figures S13 and S14, Supporting Information), presenting tunability and wavelength adaptability over a broad spectral range. The FPG demonstrated here shows a limited diffraction angle, originating from the large pixel size. For optical applications, gratings with smaller periods are desired. The resolution of LC jigsaw puzzle can be further optimized by utilizing an objective lens with larger magnification or apertures with small size. In addition, diverse nematic LCs are used to further verify the feasibility of surface reliefs in directing LCs. The resulting jigsaw puzzles show defect-free texture with the desired performance (Figure S15, Supporting Information).

Particularly, the most prominent advantage based on the LC jigsaw puzzles technique is the surprising stability with the illumination of short-wavelength light, which is completely distinct from the traditional photoalignment technique. Short-wavelength light plays a crucial role in both scientific and technological areas, such as underwater optical communications,[45,46] high-resolution microscopy,[47,48] and optical manipulation with a strong trapping force.[49,50] Therefore, the optical stability and durability of optical devices are of paramount importance from an application viewpoint. Herein, the performance of the components based on LC jigsaw puzzles is evaluated with illumination with a blue laser (457 nm) (Figure S16, Supporting Information). The results show that the FPG based on LC jigsaw puzzles remains intact with invariable diffraction performance when illuminated with an even higher intensity (over 63.66 mW cm^{-2}) and maintains its functions after at least 400 h of illumination. Furthermore, a 355-nm pulsed laser (80 kHz), with a pulse width of 15 ns and a single pulse energy of 25 μJ, is employed to evaluate the stability in UV illumination. As expected, the optical textures of uniformly orientated LCs confined by pixelated reliefs exhibit bright and dark states without arranged defects, which corroborates the satisfactory orientation stability of LCs (Figure S17, Supporting Information). In contrast, the LC arrangement based on the traditional photochemical technique is destroyed in seconds under the same illumination conditions (Figure S18, Supporting Information).

Significantly, a unique three-dimensional optical encoding technique is proposed using the polarization, wavelength, and optical mode with a single FPG. Diverse beams are coupled together to generate Gaussian and OV modes with different wavelengths by modulating the external voltages and the polarization of incident light; this promotes an ingenious optical coding method beyond traditional binary systems without complicated equipment, leading to more efficient solutions for some computations.[51] Herein, the optical encoder prototype is designed, as illustrated in Figure 3c, where 405-nm and 532-nm lasers are employed to generate single-, double- and even triple-bit ternary coding information by rationally selecting the driving voltages of the FPG and designing the incident polarization and wavelength. Specifically, the Gaussian mode denotes "0", while the vortex with a short wavelength (405 nm) is "1" and the vortex with a 532 nm wavelength is "2"; therefore, various combinations of ternary code can be obtained (Figure 3d; Figure S19, Supporting Information). Fundamentally, the three-dimensional optical encoding originates from the distinct phase retardations when the incident light passes through the LC-based FPG, so that the corresponding diffraction efficiency changes with the driving voltage (Figure 3e), endowing possibilities to achieve a versatile encoding system. As a proof of concept, four typical double-bit ternary encodings of "0, 0", "0, 1", "2, 0", and "2, 1" and triple-bit ternary encodings "2, 0, 0", "2, 0, 1", and "2, 1, 0" are experimentally implemented (Figure 3f). Moreover, the encoding bits can be increased to four and even five digits by judiciously designing the input information, i.e., the driving voltage of FPG and polarization of incident light (Figure S19, Supporting Information). Meanwhile, the encoding capacity is further enhanced by coupling extra impinged beams with distinct wavelengths, thereby holding promise in higher digitalized encoding.

Light-matter interactions have inspired many intriguing optical manipulations, such as light-driven microdrones and optical tweezers, playing crucial roles in chemistry, physics, and biology. By utilizing liquid crystal spatial light modulators (SLM), the trapping and sorting of micro-particles via holographic beams have been studied widely.[52,53] Among the practical applications, manipulation with short-wavelength light has emerged as an indispensable technique in various areas.[49,50,54] Compared with SLM, conventional planar optical elements of LCs can simplify the optical setup to achieve a compact manipulation facility but suffer from instability upon short wavelength radiation. In contrast, LC jigsaw puzzles provide satisfactory stability for optical applications and thus unlock the full potential of LCs in multiple remote non-contact particle manipulations. To further corroborate this, we demonstrate optical tweezers using a blue laser with its movement controlled in three degrees of freedom, that is, 2D motions, direction, and velocity of rotation. The optical configurations are illustrated in **Figure 4**a, and more details are given in the Experimental section. A group of silica microspheres with a diameter of 1.5 μm dispersed in water are sandwiched between two transparent microslides. After the phase modulation of the LC *q*-plate (Figure 4b), an OV beam with a wavelength of 457 nm illuminates the sample. The 2D motions of trapped particles can be realized by changing the position of the focused OV; then, different numbers of microspheres are transferred and assembled to generate diverse patterns (Figure 4c). Specifically, 11 particles are trapped and arranged as an arrowhead to visually demonstrate the control of the rotation directions. Anticlockwise and clockwise rotations can be observed with the illumination of left-handed circularly polarized (l-CP) and right-handed circularly polarized (r-CP) incident lights, respectively (Figure 4d,e; Video S3, Supporting Information). Prior works indicate that the rotation of trapped particles depends on the orbital angular momentum (OAM) transferred from light to matter;[55,56] nevertheless, the rotation velocity remains uncontrolled unless bulky modulators, such as the common spatial light modulator, are leveraged to reload the distinct OV beams. Herein, an external electric field is applied on the LC *q*-plate to judiciously regulate the phase retardation of transmitted light, triggering a controllable transformation of the manipulating beam from Gaussian to vortex mode (Figure 4f). Correspondingly, the trapped particles rotate from a static state, and the rotation velocity accelerates gradually as the driving voltage increases and then reaches the maximum as the incident beam completely transforms into the OV beam (Figure 4g; Note S6 and Video S4, Supporting Information). Consequently, the LC optical elements provide a new degree of freedom for particle manipulation, and

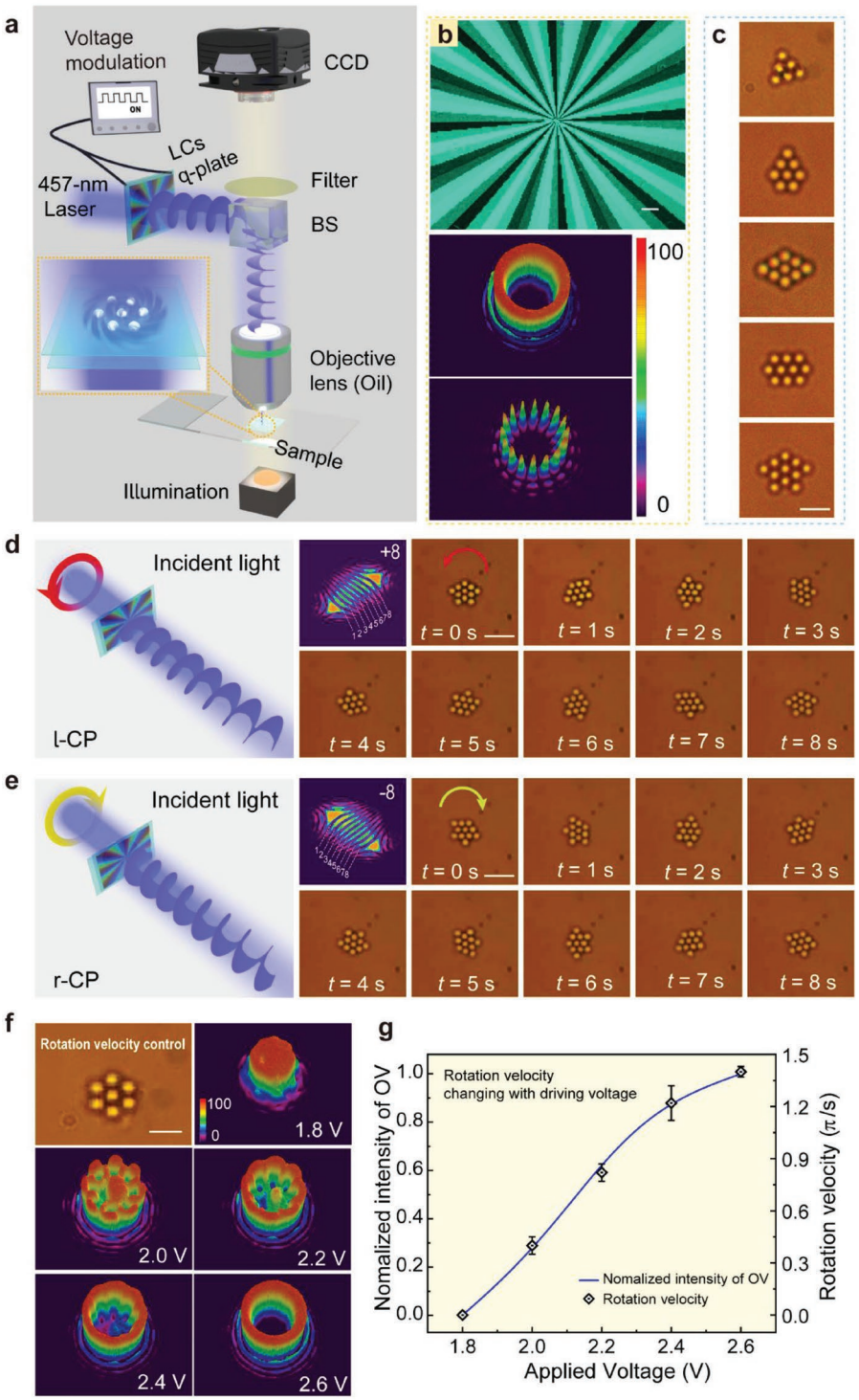

Figure 4. Optical manipulation via an LC *q*-plate based on jigsaw puzzles. a) Experimental configuration of the optical manipulation. b) Microscopy image of the *q*-plate is exhibited in the top left corner; scale bar: 200 µm. The intensity distribution of diffraction as linearly polarized incidence is shown below the microscopy image. The bottom image of the intensity distribution shows petal-shaped intensity patterns after passing through a linear polarizer, and 16 petals demonstrate that the topologic charge of the LC *q*-plate is 8 ($q = 8$). c) The diverse shapes of trapped particles. The diameter of the particles is 1.5 µm; scale bar: 4 µm. d) and e) control of the rotation directions. The intensity distribution image in the focal plane of the cylindrical lens, which reveals the converted pattern of the OV, and the number of dark stripes and the stripe tilt direction indicate topological charges of +8 (d) and −8 (e), respectively. Anticlockwise (d) and clockwise (e) rotation of arrowhead-shaped particles at different time points (Video S3, Supporting Information). The scale bars are 6 µm. f) Control of the rotation velocity via an external electric field. The micrograph shows the particles trapped by the OV beam ($q = +8$), and the intensity distribution images reveal the transformation of the OV beam generated by the LC optical puzzle at different applying voltages. g) Dependency of the rotation velocity on the applied voltage (Video S4, Supporting Information). The scale bar is 3 µm.

a stable, compact, and versatile particle manipulation system with dynamic tunability is achieved. Essentially, the tunability of LCs can offer a dynamically switchable structured light field to the optical manipulations, and the movement of trapped objects can be regulated via the external stimuli on the LC component. Thus, the excessive switching process to generate diverse phase distributions is avoided, which is distinct from traditional optical nano- and mesoscale manipulations. Moreover, as confirmed by the optical trapping test, the elements based on LC jigsaw puzzles, which are sealed well with epoxy glue and stored in a thermostatically controlled environment at 25 °C, can maintain their functions after storage for > 15 months (Video S5, Supporting Information), showing reliable durability. We believe that the tunability and durability make LC jigsaw puzzles a promising choice for compact, accurate, and multifunctional optical manipulations, providing more possibilities in optical cooling,[57] particle sorting,[53] biological detection,[50] and so on.

The Airy beam has attracted sustained interest and has made impressive progress owing to its unique features of nondiffraction, transverse acceleration, and self-healing.[58–61] Previously reported Airy beam generators based on LCs show merits of tunability with compact size; however, the poor stability upon short wavelength irradiation impedes practical applications. Herein, a hologram to generate an Airy beam was achieved via LC jigsaw puzzles (**Figure 5**a), and all demonstrations of the Airy beam were carried out using a 457 nm blue laser to confirm the stability of the LC Airy phase mask. The Airy beam can be reversibly switched to a Gaussian beam with external voltages (Figure 5b; Video S6, Supporting Information) and exhibits polarization-controllable switching behaviors (Figure 5c; Figure S20a, Supporting Information), which may inspire corresponding applications, such as dynamically tunable or chirality-selective optical manipulations.[62,63] Furthermore, the transverse deflections at certain propagation distances are experimentally detected (Figure 5d; Figure S20b, Supporting Information), where each branched Airy beam tends to deviate from its initial direction when propagating in the space, implying the transverse acceleration property of the Airy beam. In addition, when a pentagon-shaped mask is inserted into the light path to obstruct the main lobe of the output Airy beam, the main lobe is reconstructed gradually during propagation to distance, indicating the self-healing ability of a nondiffracting field configuration (Figure 5e; Video S7, Supporting Information). In contrast, when switching to a Gaussian beam, the partially obscured light field could not be reconstructed. Such unique features of the Airy beam provide a new view on space explorations where the self-healing property enables the Airy beam to reconstruct the profile during the propagation in turbulence. Moreover, as light with wavelengths in the range of 425–475 nm experiences negligible attenuation when propagating through clear water, we envision that the proposed Airy phase mask has great potential in underwater communications and adaptive optics.

3. Conclusion

We have reported a strategy to program the self-organization of soft matter, enabling LC jigsaw puzzles as programmable soft photonics via pixelated holographic surface reliefs. A top-down processing of digitalized holographic lithography is developed to achieve the desired reliefs, and the orientations of nanoscale LC directors can be customized by programming the subwavelength topography, revealing a delicate harmonization between the LC self-assembling order and the anchoring condition of holographic reliefs. Impressively, contrary to traditional photochemical techniques, the proposed approach can provide satisfactory stability and durability, thereby expanding the potential applications of LCs in the short wavelength range. The versatile fabrication of LC jigsaw puzzles overcomes the limited scale in defining LC architectures and enables either macroscopic patterns or microstructures, further promoting fascinating prototypes of tunable soft photonics with exciting practicabilities, such as the switchable E-tag, active tunable structured light, multidimensional optical encoding and manipulations presented herein. We anticipate that this work will open new avenues in programming soft material and relevant systems, thereby providing a promising platform for diverse areas such as photonics, physics, biology, and life sciences.

4. Experimental Section

Materials: A commercial positive photoresist RZJ-390PG (SZ Ruihong Electronic Chemicals Co., LTD.) was used to generate the holographic relief structure. The commercial LC 5CB exhibited a nematic state in a temperature range of 20.6 °C to 36.8 °C with a birefringence $\Delta n = 0.180$ at 23 °C and a clear point ≈36.8 °C (provided by Slichem Co., Ltd., China, Note S2, Supporting Information).

Fabrication of the Holographic Relief Structure: Indium-tin-oxide (ITO) glasses (2.1 × 2.3 cm^2) were ultrasonically bathed and UV–ozone cleaned, and the positive photoresist was spin-coated on the ITO glasses. A 355 nm pulsed laser (Advanced Optowave Corporation. maximum repetition rate: 80 kHz, pulse width: 15 ns, single pulse energy: 25 µJ) was used for exposure, and the holographic microimage of the one-dimensional grating was recorded by a photoresist. The objective lens was 20×. The space frequency range of the diffractive optical element in the digital holography lithography system was 60 line mm^{-1} (for the principle of the digital holography lithography system, see Note S1, Supporting Information for details). A collimated and uniform pulsed UV laser beam was incident upon a 4f imaging system with a diffractive optical element (DOE) situated between the two Fourier lenses. Then, a holographic image of the DOE was collected and written into the recording medium via an objective lens. With the aid of an autofocusing system and a precision mechanical stage, pixelated holographic reliefs were distributed across the sample as the peculiar topography to complete the soft optical puzzle. When writing pixels with uniform direction, a matrix mode was used, the repetition rate of the pulse laser was 1 kHz, and the photoresist would be exposed line by line. As it required time to return to the next line, it took ≈5 min to accomplish 10 mm × 10 mm regions, which contained 200 × 200 pixels with 50 µm side length and uniform direction. When writing pixels for a customized image with different orientations, a step mode was used, which employed a pixel-by-pixel discrete scan approach, and the pixels with the same orientation would be written first. Both of the two writing modes employed one-short exposure in each pixel, and the precision mechanical stage could provide accurate control of the relief positions. The quick response (QR) code demonstrated in Figure 2b contained 200 × 200 pixels with a resolution of 25 µm, and it took ≈67 min to accomplish it. After exposure, a 0.65% NaOH solution was used for development to remove the photoresist of the exposed part. Then, the specimen was baked at 130 °C for 5 min before the fabrication of the LC cell. The cell gaps of all the samples demonstrated in this manuscript were controlled with 5 µm spacers. The LC material was

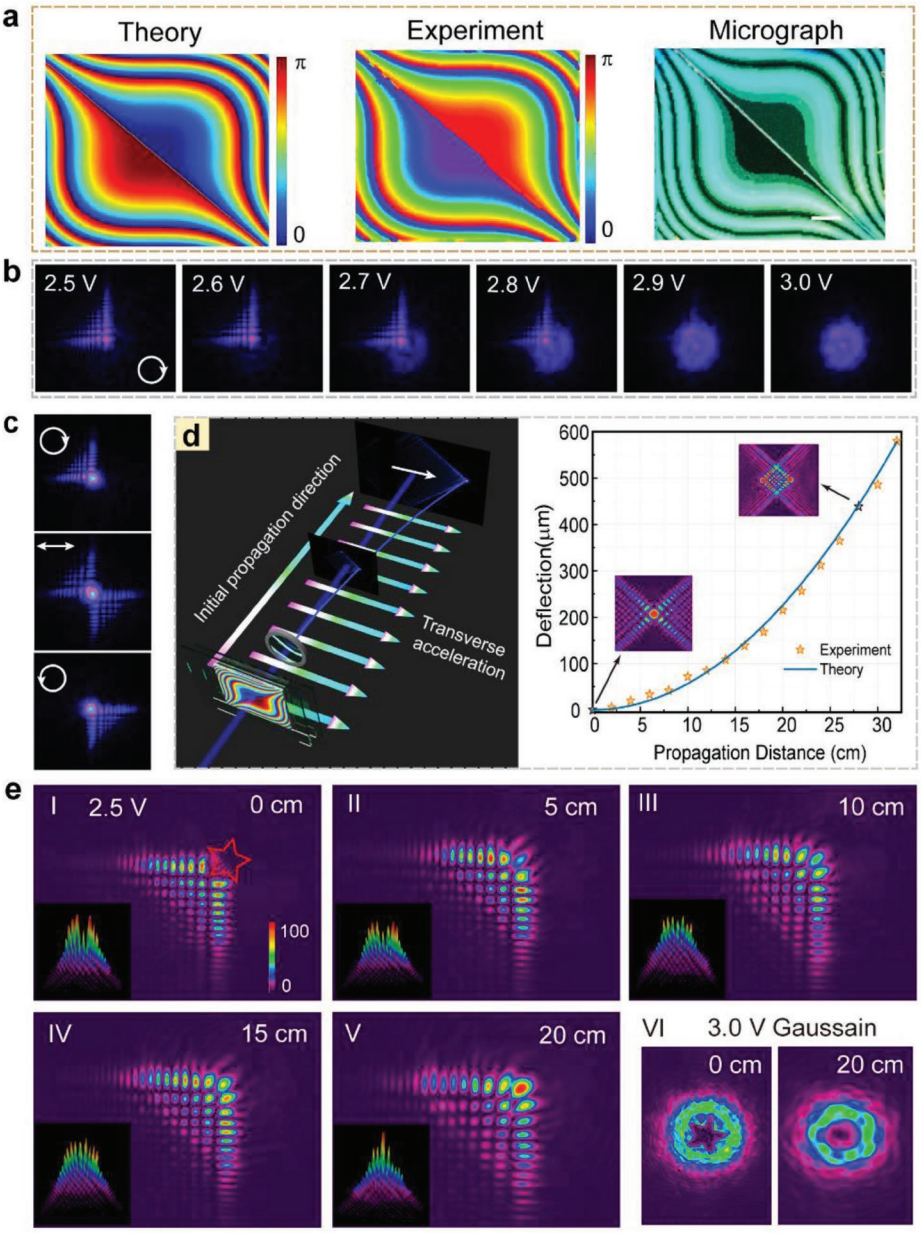

Figure 5. Planar optical elements based on LC jigsaw puzzles to generate an Airy beam. a) The theoretical design, experimental data, and micrograph of the Airy phase puzzle. Scale bar: 200 μm. b) The electrical tunability of LC Airy phase mask. The Airy beam can be reversibly switched to a Gaussian beam with external voltages, and the energy distribution varies correspondingly. c) The polarization-controllable switching behaviors of LC Airy phase mask. The incident polarizations are labeled in the images; clockwise/counterclockwise indicates left/right circularly polarized light. d) Schematic diagram and experimental detection of self-acceleration. The transverse deflections (x) can be obtained from the distance between the two main lobes (d), where $x = d/2$. e) The self-healing property of the Airy beam. The main lobe is blocked by a pentagram barrier. Observed intensity profile during propagation at: I) 0 cm, II) 5 cm, III) 10 cm, IV) 15 cm, and V) 20 cm; the driving voltage is 2.5 V. VI) When the driving voltage is 3.0 V, the Gaussian beam without the self-healing property remains incomplete.

capillary-filled into the photopatterned cell at 45 °C and slowly cooled to room temperature.

Illustration of the Pixelated Reliefs: The pixel size was controlled by adjusting the aperture in the lithography setup. Herein, micro-square pieces with large sizes were employed in the macroscopic patterns, while small-sized pieces were appropriate in planar optics. The maximum size of the pixelated micro-square pieces was 50 μm × 50 μm, and the resolution of the TN LC cell demonstrated in Figure 2a was 50 μm; the macroscopic patterns in Figure 2b,d,e were constructed with the 25 μm × 25 μm pieces. The Pancharatnam Berry (PB) phase planar optical elements were constructed with the 16 μm × 16 μm micro-square pieces.

Feasibility of the Holographic Surface Reliefs in Directing Nematic LCs: Two commercial nematic LCs, E7 (birefringence Δn = 0.199 at 20 °C, clear point 58 °C, provided by HCCH, China) and TEB300 (birefringence Δn = 0.166 at 20 °C, clear point 63 °C, provided by Slichem Co., Ltd., China) were employed to further confirm the feasibility of the holographic surface reliefs in directing the self-organization of nematic LCs. Both macroscale and microscale optical jigsaw puzzles were

solved. The POMs of the nematic LC jigsaw puzzles show defect-free texture, and the diffractions of FPGs present typical OVs with electric-controllable and polarization-dependent switching behaviors (Figure S15, Supporting information). Hence, the proposed holographic reliefs showed reliable feasibility in directing nematic LCs.

Optical Manipulation System: The light emitted from a 457-nm laser (100 mW), a polarizer, and a 1/4 λ wave plate (which were not shown in the schematic diagram of the experimental configuration) was used to adjust the polarization of the incident beam. The *q*-plate LC phase puzzles were illuminated to generate OV beams. After going through the beam splitter (BS) and an oil-immersion microscope objective (Nikon, 100×, NA = 1.35), a tightly focused OV beam illuminated the particle cell. Silica microspheres (1.5 µm diameter) in water solution were sandwiched between two thin microslide glass plates as the sample chamber. A white lamp was used as the illumination source. The manipulations were captured by a charge-coupled device (CCD) camera.

Characterizations: All experiments were performed at room temperature in an ambient environment. POM textures were observed by a polarized optical microscope (LVPOL 100, Nikon) and recorded by a CCD camera (DS-U3, Nikon) with two crossed linear polarizers in transmission mode. The display patterns and diffraction patterns from geometric phase elements were captured by a digital camera (EOS 70D, Canon, Japan). The intensity distribution of the optical vortices and Airy beam were detected and simultaneously analyzed by a CCD beam profiler system (SP620U, Spiricon). The azimuthal anchoring energy was tested via the twist angle method (see Supporting Information Note S2 for details).

Supporting Information

Supporting Information is available from the Wiley Online Library or from the author.

Acknowledgements

Y.W., C.Y., and W.H. contributed equally to this work. The authors acknowledge the support from the National Key Research and Development Program of China (SQ2022YFA1200117), the National Science Foundation of China (grant nos. 61822504, 62275081, 51873060, and 62035008), Innovation Program of Shanghai Municipal Education Commission, Scientific Committee of Shanghai (2021-01-07-00-02-E00107), "Shuguang Program" of Shanghai Education Development Foundation, Shanghai Municipal Education Commission (21SG29), and Jiangsu Innovation Team Program.

Conflict of Interest

The authors declare no conflict of interest.

Data Availability Statement

The raw data that support the findings of this study are available from the corresponding author upon reasonable request.

Keywords

jigsaw puzzles, liquid crystals, planar optics, soft materials, stability

Received: December 8, 2022
Revised: January 23, 2023
Published online: February 17, 2023

[1] A. Chworos, I. Severcan, A. Y. Koyfman, P. Weinkam, E. Oroudjev, H. G. Hansma, L. Jaeger, *Science* **2004**, *306*, 2068.
[2] J. Deng, X. Kuang, R. Liu, W. Ding, A. C. Wang, Y. C. Lai, K. Dong, Z. Wen, Y. Wang, L. Wang, H. J. Qi, T. Zhang, Z. L. Wang, *Adv. Mater.* **2018**, *30*, 1705918.
[3] C. Coulais, E. Teomy, K. de Reus, Y. Shokef, M. van Hecke, *Nature* **2016**, *535*, 529.
[4] P. Dieleman, N. Vasmel, S. Waitukaitis, M. van Hecke, *Nat. Phys.* **2019**, *16*, 63.
[5] C. Harrison, C. M. Stafford, W. Zhang, A. Karim, *Appl. Phys. Lett.* **2004**, *85*, 4016.
[6] J. J. Huang, L. Y. Zhang, Y. Q. Yang, *Opt. Express* **2011**, *19*, 814.
[7] A. V. Kildishev, A. Boltasseva, V. M. Shalaev, *Science* **2013**, *339*, 1232009.
[8] L. Liu, X. Zhang, M. Kenney, X. Su, N. Xu, C. Ouyang, Y. Shi, J. Han, W. Zhang, S. Zhang, *Adv. Mater.* **2014**, *26*, 5031.
[9] Z. Zheng, H. Hu, Z. Zhang, B. Liu, M. Li, D.-H. Qu, H. Tian, W.-H. Zhu, B. L. Feringa, *Nat. Photonics* **2022**, *16*, 226.
[10] E. Song, J. Li, S. M. Won, W. Bai, J. A. Rogers, *Nat. Mater.* **2020**, *19*, 590.
[11] J. Zhang, Y. Guo, W. Hu, R. H. Soon, Z. S. Davidson, M. Sitti, *Adv. Mater.* **2021**, *33*, 2006191.
[12] B. Liu, C. L. Yuan, H. L. Hu, H. Wang, Y. W. Zhu, P. Z. Sun, Z. Y. Li, Z. G. Zheng, Q. Li, *Nat. Commun.* **2022**, *13*, 2712.
[13] H. K. Bisoyi, Q. Li, *Chem. Rev.* **2022**, *122*, 4887.
[14] X. Zhang, Y. Xu, C. Valenzuela, X. Zhang, L. Wang, W. Feng, Q. Li, *Light: Sci. Appl.* **2022**, *11*, 223.
[15] H. K. Bisoyi, T. J. Bunning, Q. Li, *Adv. Mater.* **2018**, *30*, 1706512.
[16] S. H. Paek, C. J. Durning, K. W. Lee, A. Lien, *J. Appl. Phys.* **1998**, *83*, 1270.
[17] Z. He, Y. H. Lee, R. Chen, D. Chanda, S. T. Wu, *Opt. Lett.* **2018**, *43*, 5062.
[18] A. Suh, D. K. Yoon, *Sci. Rep.* **2018**, *8*, 9460.
[19] J. Kim, Y. Li, M. N. Miskiewicz, C. Oh, M. W. Kudenov, M. J. Escuti, *Optica* **2015**, *2*, 958.
[20] Z. He, Y. H. Lee, D. Chanda, S. T. Wu, *Opt. Express* **2018**, *26*, 21184.
[21] Z. G. Zheng, C. L. Yuan, W. Hu, H. K. Bisoyi, M. J. Tang, Z. Liu, P. Z. Sun, W. Q. Yang, X. Q. Wang, D. Shen, Y. Li, F. Ye, Y. Q. Lu, G. Li, Q. Li, *Adv. Mater.* **2017**, *29*, 1703165.
[22] P. Chen, L. L. Ma, W. Hu, Z. X. Shen, H. K. Bisoyi, S. B. Wu, S. J. Ge, Q. Li, Y. Q. Lu, *Nat. Commun.* **2019**, *10*, 2518.
[23] S. U. Kim, Y. J. Lee, J. Liu, D. S. Kim, H. Wang, S. Yang, *Nat. Mater.* **2022**, *21*, 41.
[24] H. Ren, Y.-H. Fan, S.-T. Wu, *Appl. Phys. Lett.* **2003**, *83*, 1515.
[25] M. Honma, T. Nose, S. Yanase, R. Yamaguchi, S. Sato, *Opt. Express* **2009**, *17*, 10998.
[26] J. Oh, K. Lee, Y. Park, *Laser Photonics Rev.*. **2021**, *16*, 2100559.
[27] W. Hu, A. Srivastava, F. Xu, J.-T. Sun, X.-W. Lin, H.-Q. Cui, V. Chigrinov, Y.-Q. Lu, *Opt. Express* **2012**, *20*, 5384.
[28] V. G. Chigrinov, V. M. Kozenkov, H.-S. Kwok, *Photoalignment of Liquid Crystalline Materials: Physics and Applications*, Wiley, Hoboken, NJ, USA **2008**.
[29] S.-J. Sung, H.-T. Kim, J.-W. Lee, J.-K. Park, *Synth. Met.* **2001**, *117*, 277.
[30] Z.-X. Zhong, X. Li, S. H. Lee, M.-H. Lee, *Appl. Phys. Lett.* **2004**, *85*, 2520.
[31] M. Rafayelyan, G. Agez, E. Brasselet, *Phys. Rev. A* **2017**, *96*, 043862.
[32] Y. Wang, C. Xu, A. Kanazawa, T. Shiono, T. Ikeda, Y. Matsuki, Y. Takeuchi, *Liq. Cryst.* **2010**, *28*, 473.
[33] C. J. Newsome, M. O'Neill, R. J. Farley, G. P. Bryan-Brown, *Appl. Phys. Lett.* **1998**, *72*, 2078.
[34] C. H. Lee, H. Yoshida, Y. Miura, A. Fujii, M. Ozaki, *Appl. Phys. Lett.* **2008**, *93*, 173509.
[35] J. Yan, Q. Li, K. Hu, *J. Appl. Phys.* **2013**, *114*, 153104.
[36] I. Nys, J. Beeckman, K. Neyts, *Adv. Opt. Mater.* **2018**, *6*, 1800070.
[37] J. Cattle, P. Bao, J. P. Bramble, R. J. Bushby, S. D. Evans, J. E. Lydon, D. J. Tate, *Adv. Funct. Mater.* **2013**, *23*, 5997.

[38] Y. Cui, R. S. Zola, Y.-C. Yang, D.-K. Yang, *J. Appl. Phys.* **2012**, *111*, 063520.
[39] Y. Choi, H. Yokoyama, J. S. Gwag, *Opt. Express* **2013**, *21*, 12135.
[40] J. S. Gwag, J. H. Kwon, M. Oh-e, J.-i. Niitsuma, M. Yoneya, H. Yokoyama, *Appl. Phys. Lett.* **2009**, *95*, 103101.
[41] X. M. Goh, Y. Zheng, S. J. Tan, L. Zhang, K. Kumar, C. W. Qiu, J. K. Yang, *Nat. Commun.* **2014**, *5*, 5361.
[42] J. Oh, D. Baek, T. K. Lee, D. Kang, H. Hwang, E. M. Go, I. Jeon, Y. You, C. Son, D. Kim, M. Whang, K. Nam, M. Jang, J. H. Park, S. K. Kwak, J. Kim, J. Lee, *Nat. Mater.* **2021**, *20*, 385.
[43] V. Y. Bazhenov, M. S. Soskin, M. V. Vasnetsov, *J Mod Opt* **2007**, *39*, 985.
[44] Q. Zhan, *Adv. Opt. Photonics* **2009**, *1*, 1.
[45] G. M. Hale, M. R. Querry, *Appl. Opt.* **1973**, *12*, 555.
[46] J. Baghdady, K. Miller, K. Morgan, M. B. S. Osler, R. Ragusa, W. Z. Li, B. M. Cochenour, E. G. Johnson, *Opt. Express* **2016**, *24*, 9794.
[47] W. T. Chen, M. Khorasaninejad, A. Y. Zhu, J. Oh, R. C. Devlin, A. Zaidi, F. Capasso, *Light Sci Appl* **2017**, *6*, e16259.
[48] D. Y. Guo, C. W. Chen, C. C. Li, H. C. Jau, K. H. Lin, T. M. Feng, C. T. Wang, T. J. Bunning, I. C. Khoo, T. H. Lin, *Nat. Mater.* **2020**, *19*, 94.
[49] D. E. Smalley, E. Nygaard, K. Squire, J. Van Wagoner, J. Rasmussen, S. Gneiting, K. Qaderi, J. Goodsell, W. Rogers, M. Lindsey, K. Costner, A. Monk, M. Pearson, B. Haymore, J. Peatross, *Nature* **2018**, *553*, 486.
[50] D. Cao, C. Y. Li, Y. F. Kang, Y. Lin, R. Cui, D. W. Pang, H. W. Tang, *Biosens. Bioelectron.* **2016**, *86*, 1031.
[51] A. Bocharov, M. Roetteler, K. M. Svore, *Phys. Rev. A* **2017**, *96*, 012306.
[52] R. Paez-Lopez, U. Ruiz, V. Arrizon, R. Ramos-Garcia, *Opt. Lett.* **2016**, *41*, 4138.
[53] M. Chen, S. Huang, X. Liu, Y. Chen, W. Shao, *Appl. Phys. B* **2019**, *125*, 184.
[54] Z. Gong, Y. L. Pan, C. Wang, *Rev. Sci. Instrum.* **2016**, *87*, 103104.
[55] H. He, M. E. Friese, N. R. Heckenberg, H. Rubinsztein-Dunlop, *Phys. Rev. Lett.* **1995**, *75*, 826.
[56] M. Padgett, R. Bowman, *Nat. Photonics* **2011**, *5*, 343.
[57] M. A. Clifford, J. Arlt, J. Courtial, K. Dholakia, *Opt. Commun.* **1998**, *156*, 300.
[58] G. A. Siviloglou, J. Broky, A. Dogariu, D. N. Christodoulides, *Phys. Rev. Lett.* **2007**, *99*, 213901.
[59] R.-P. Chen, C.-F. Yin, X.-X. Chu, H. Wang, *Phys. Rev. A* **2010**, *82*, 043832.
[60] J. Wang, X. Hua, C. Guo, W. Liu, S. Jia, *Optica* **2020**, *7*, 790.
[61] N. K. Efremidis, Z. Chen, M. Segev, D. N. Christodoulides, *Optica* **2019**, *6*, 686.
[62] J. Baumgartl, M. Mazilu, K. Dholakia, *Nat. Photon.* **2008**, *2*, 675.
[63] G. Tkachenko, E. Brasselet, *Nat. Commun.* **2014**, *5*, 4491.